THE ASTROPHYSICAL JOURNAL, 327:570–583, 1988 April 15

QUASAR IONIZATION OF LYMAN-ALPHA CLOUDS: THE PROXIMITY EFFECT, A PROBE OF THE ULTRAVIOLET BACKGROUND AT HIGH REDSHIFT

STANISLAW BAJTLIK,[1] ROBERT C. DUNCAN, AND JEREMIAH P. OSTRIKER
Princeton University Observatory
Received 1987 June 1; accepted 1987 October 6

ABSTRACT

We study the distribution of lines in the Lyα forests in quasar spectra, using spectral data from 19 quasars with emission-line redshifts $1.7 < z_Q < 3.8$. The number density of Lyα lines generally increases with redshift z, but there exists a countervailing trend of diminishing number density within individual quasar spectra as $z \to z_Q$.

We give evidence that this countervailing trend is due to enhanced ionization of Lyα clouds by the bright, nearby quasars in whose spectra they are observed (the "proximity effect"). We develop a quantitive physical model for this effect, and using a variety of statistical tests, we show that the model fits the data; furthermore, we infer the background of ionizing photons at large z by optimizing the fit. Assuming our model is correct, this represents the first physical *measurement* of the high-z UV background. Roughly speaking, the background radiation intensity is found to be *constant* for $1.7 < z < 3.8$ and equal to

$$\log J_\nu = -21.0 \pm 0.5 ,$$

where J_ν is the Lyman-limit intensity in units ergs cm^{-2} s^{-1} Hz^{-1} sr^{-1}. This is larger than the integrated UV emission of observed quasars at $z > 3$, so there must exist appreciable sources of ionizing photons other than quasars at high z, or else many high-z quasars must be obscured by intervening dust.

The redshift evolution index for the general Lyα cloud population, γ, is found to be systematically larger than otherwise when the proximity effect is correctly taken into account. In our sample, we find $\gamma = 2.36 \pm 0.40$.

If our conclusions are confirmed by studies using a larger statistical base, then the "proximity effect" can be used as a powerful tool to measure *locally* the ionizing flux emitted by high-redshift objects. It could be used to check if BL Lac objects emit strongly beamed radiation as predicted by models, to study stochastic variations in OVV quasars, and to measure quasar flux amplification by gravitational lenses.

Subject headings: cosmology — quasars — ultraviolet: spectra

I. INTRODUCTION

The multitudinous absorption lines seen blueward of Lyman-α emission in QSO spectra are generally interpreted as being due to clouds of primordial material, distributed in space on the largest observable scales. The line distribution in this Lyα forest has been widely studied since Peterson (1978), showed that the numbers vary as a steep function of redshift, and Sargent *et al.* (1980) showed that the low metal abundances, large numbers, and lack of clustering of the Lyα clouds imply that they are probably unassociated with galaxies or quasars. These Lyα clouds are far more numerous than quasars or metal line absorption systems, and are seen to a much larger redshift than galaxies. Thus they potentially can convey more information about the universe at moderate redshift than any other type of astronomical object so far observed. Insofar as they seem to be quite chemically pure, an analysis of their properties may tell us something about the universe before or during the epoch of galaxy formation. Some of their properties are by now fairly well established.

The number of clouds per unit redshift of a given equivalent width increases with redshift. But empirical fits of the observed cloud numbers to a power law distribution

$$\frac{d\mathcal{N}}{dz} = \mathcal{A}_0(1+z)^\gamma \qquad (1)$$

by many different authors have produced a confusing range of estimates of the index γ, as described by Murdoch *et al.* (1986, hereafter MHPB). As shown by MHPB, this confusion has been caused—in part, at least— by the so-called inverse effect in the cloud distribution: the cloud number density rises less rapidly with redshift within the spectra of an individual QSO, as one approaches the QSO, than in an ensemble of QSO spectra at the same redshift. This effect, discovered by Carswell *et al.* (1982) and studied by MHPB and Tytler (1987), has not yet been convincingly explained. Tytler (1987), for example, puts forward several possible explanations for the effect, but finds no clear reason to chose one over another.

In this paper we address the question: can the "inverse effect," or as we prefer to call it, the "proximity effect," be attributed to photoionization of clouds by the bright QSOs in whose spectra they are observed? In § II we describe our data set (assembled from the published literature) and show that deviations from equation (1) in individual QSO spectra are correlated with intrinsic QSO luminosity. In § III we describe a simple photoionization model for the "proximity effect." In § IV we show how this model confronts the observations. A variety of independent tests provide corroborating evidence, but of course we cannot exclude the possibility that another theoretical model would fit as well. Also in § IV we discuss the bounds we find on the general background of ionizing photons at high redshift if the model is correct. This ionizing background is presumably due to the integrated UV emission of all quasars. In § V we investigate how time variations in quasar

[1] On leave from the Copernicus Astronomical Center, Polish Academy of Sciences, Warsaw, Poland.

intrinsic luminosities may affect the proximate Lyα line distribution

Since the QSO absorption-line data now available are very limited compared to what is observationally possible, our emphasis throughout will be on *how* to take the "proximity effect" into account when analyzing the cloud distribution, and what we can learn from this effect, rather than on making definitive statements about the distribution. Furthermore we emphasize that the data we utilize for this study are not the spectra themselves but rather the line lists assembled by the various observational teams from analyses of their data. Since line-blending, confusion between Lyα and other lines, instrumental effects, and a host of other complexities can introduce error in the identification and measurement of Lyα lines, the line lists must be treated with some caution. Jenkins (1988) is attempting to analyze on a fundamental basis the mapping between cloud properties and observed spectra. We in this paper, while exercising all due caution, have no choice but to accept the published line lists as real after we have edited out the parts believed to be least reliable.

In § VI we discuss some of the issues raised by our present results, and how these issues may be resolved using the larger and more homogeneous data base that we hope will be available in the future.

II. THE DATA SAMPLE

High-resolution spectra of 19 QSOs with emission-line redshifts z_Q ranging from 1.73 to 3.78 comprise our data sample (see Table 1). In our statistical study of lines, we count all lines with rest frame equivalent widths greater than 0.36 Å, except for those that belong to metal-line systems, which presumably represent a distinct group of objects (Sargent *et al.* 1980). Possible inhomogeneities in the data due to different observers and different data reduction techniques are minimized by taking an equivalent width cutoff that is well above the putative threshold of completeness. In our sample, we utilized only 470 lines out of about 1500 listed. Neverthless, low-level systematic inhomogeneities may remain due to line crowding.

Absolute spectrophotometry was available for most of the QSOs in our sample, from which we estimated the intrinsic continuum intensity at the Lyman limit (Table 1). For eight of the QSOs, we have had to rely on the empirical fitting formula of Tytler (1987)

$$\log_{10} f_\nu (1 + z_Q)^{-1} = -0.4(m_\nu - k_\nu) - 20.09 , \qquad (2)$$

which relates the Lyman-limit flux density f_ν to the visual magnitude with K-corrections, and is accurate to $\sim 40\%$.

Since we have used all complete, published line lists, our

TABLE 1

QSO ABSORPTION SPECTRUM DATA SAMPLE

QSO	z_Q	z_L[a]	$\mathcal{N}_{obs}$[b]	F_ν[c]	Spectrum Reference	Spectrophotometry Reference
1115+080.....	1.725	1.682	2	0.57	1	12
0002+051.....	1.899	1.718	4	4.1	1	13
0119−046.....	1.937	1.683	11	3.4	2	14
0421+019.....	2.051	1.712	8	2.9	1	14
1101−264.....	2.143	1.856	7	6.2	3	15
0122−380.....	2.181	1.974	9	4.9	4	14
1225+317.....	2.20	1.70*	14	11.0	5	16
0237−233.....	2.223	2.069	5	4.4	5	14
1623+269.....	2.518	2.257	14	2.5	6	14
1623+268.....	2.605	2.252	18	0.38	6	14
0453−423.....	2.656	2.203	33	3.3	5	14
0100+130.....	2.69	2.11*[d]	14	7.1	5	17
0002−422.....	2.763	2.172*	33	1.5	5	18
0528−250.....	2.765	2.174*	35	1.6	7	19
0805+046.....	2.877	2268*	42	1.5	8	14
0420−388.....	3.12	2.47*[e]	52	3.4	9	18
2126−158.....	3.28	2.61*	42	4.2	5	17
1442+101.....	3.54	2.82*	66	2.5	10	17
2000−330.....	3.783	3.032*[f]	61	3.8	11	14

[a] The lowest redshift at which we counted Lyα lines. For most QSOs this is the minimum z at which the published line lists are complete. Asterisks (*) indicate values of z_L corresponding to the onset of Lyβ lines.

[b] Total number of lines counted.

[c] QSO continuum flux density measured at the observed frequency of the Lyman limit, in units 10^{-27} ergs cm^{-2} s^{-1} Hz^{-1}. Small corrections were made for the absorption of intervening material (Oke and Korycansky 1982; Steidel and Sargent 1987). Typical uncertainty in f_ν is $\sim 30\%$.

[d] Redshift interval 2.262–2.362 is excluded because of a strong absorption feature (probably damped Lyα; see Wolfe 1987).

[e] Redshift interval 3.079–3.100 is excluded.

[f] Redshift interval 3.157–3.204 is excluded.

REFERENCES.—(1) Young, Sargent, and Boksenberg 1982; (2) Sargent, Young, and Boksenberg 1982; (3) Carswell *et al.* 1984; (4) Carswell *et al.* 1982; (5) Sargent *et al.* 1980; (6) Sargent, Young, and Schneider 1982; (7) Morton *et al.* 1980; (8) Chen *et al.* 1981; (9) Atwood, Baldwin, and Carswell 1985; (10) Peterson *et al.* 1984; (11) Hunstead *et al.* 1986; (12) The *IUE* flux from Green *et al.* 1980 has been reduced by a lens amplification factor of 8.7, from Young *et al.* 1981; (13) Bechtold *et al.* 1984; (14) Flux density from Tytler's 1987 empirical formula (eq. [2]). K-corrections are from Evans and Hart 1977. Magnitudes are from Hewitt and Burbidge 1987. (15) Boksenberg and Snijders 1981; (16) Snijders, Pettini, and Boksenberg 1981; (17) Oke and Korycansky 1982; (18) Smith *et al.* 1981; (19) Tytler 1987.

sample is essentially the same as that of Tytler (1987). Like Tytler, we have omitted the BL Lac object 0215+015 (Blades *et al.* 1985; MHPB) because of its great variability. We differ from Tytler, however, in several values of f_ν. (Our interpretation of the published spectrophotometry data apparently differs from his for a few quasars.) We verified Tytler's main results; we will discuss these in § V. Here we consider a question that Tytler did not address: Is there a correlation between intrinsic QSO luminosity and deviations from the general distribution, equation (1)?

To address this let us consider the quantity

$$\Delta\mathcal{N} \equiv \left[\mathcal{A}_0 \int_{z_Q-\Delta z}^{z_Q} (1+z)^\gamma dz\right] - \mathcal{N}(\Delta z)\,, \qquad (3)$$

where $\mathcal{N}(\Delta z)$ is the number of lines observed in a redshift interval Δz blueward of z_Q. $\Delta\mathcal{N}$ directly measures the defect in the number of lines near a quasar compared to that expected on the basis of the power-law fit (eq. [1]) to the ensemble of all quasars. The fact that for most quasars $\Delta\mathcal{N} > 0$ is a quantitative measure of the proximity effect. By considering only $z > z_Q - \Delta z$ in equation (3) we seek to reduce statistical noise. We set $\Delta z = 0.15$, which corresponds to an approximate luminosity distance from the quasar

$$r_L \approx 450 h_0^{-1}(1+z_Q)^{-2.5}\ \mathrm{Mpc}\,,$$

for $\Omega = 1$, where h_0 is the present Hubble constant in units 100 km s^{-1} Mpc^{-1}. It is difficult to imagine any physical effect associated with a quasar extending over a greater distance. For now, we assume that $\gamma = 2.4$ and $\mathcal{A}_0 = 3.0$, based on a preliminary fit of equation (1) to our 19 quasar data sample, after we have removed the $(z_Q - \Delta_z, z_Q)$ interval in each spectrum. (These values of γ and $\mathcal{A}_0$ are very close to our more careful determinations to come.)

In Figure 1 we plot $\Delta\mathcal{N}$ for each quasar versus the intrinsic QSO luminosity at the Lyman limit,

$$L_\nu = 4\pi d_L^2 f_\nu (1+z_Q)^{-1}\,. \qquad (4)$$

The factor $(1+z_Q)^{-1}$ in this equation is a bandwidth correction; d_L is the luminosity distance to Earth. The error bars in Figure 1 are set equal to $\pm[\mathcal{N}(\Delta z)]^{1/2}$. Although noisy, Figure 1 shows a definite positive correlation: all seven largest L_ν points lie $\sim 1\ \sigma$ or more above the axis, with three points more than $2\ \sigma$ above, and nowhere else on the graph do any two consecutive points do this. We can quantify this tendency for the most luminous quasars to show the largest line-number defect as follows: the average defect of the nine most luminous quasars is $\overline{\Delta\mathcal{N}} = 3.26 \pm 0.54$; whereas for the 10 faintest quasars, $\overline{\Delta\mathcal{N}} = 1.30 \pm 0.53$. The probability of such a large difference occurring by chance is only 7.9%.

Since there is a weak correlation between L_ν and z_Q in our quasar sample (correlation coefficient $\xi = 0.354$), one might suspect that the above result is due simply to the fact that $\Delta\mathcal{N}$ increases with z_Q. To resolve this question, we must use somewhat more sophisticated statistical tests (see Figs. 7 and 8 in § IV). But first, we devise a quantitative physical model for the proximity effect with which to compare the data.

III. PHOTOIONIZATION MODELS AND THE UV BACKGROUND

We now consider the photoionization of Lyα clouds near bright quasars. Although the thermodynamic history of the Lyα clouds is controversial, in almost all models the clouds are highly ionized by the general background of UV photons. This implies that the neutral hydrogen density in a cloud is inversely proportional to the ionizing flux impingent on it (neglecting weak temperature-dependent effects). In particular, for a given cloud near a bright quasar, the H I column density is

$$N = N_0(1+\omega)^{-1}\,, \qquad (5)$$

where N_0 is what the column density *would* have been if there had been no nearby quasar, and

$$\omega = \frac{F_\nu^Q}{4\pi J_\nu}\,. \qquad (6)$$

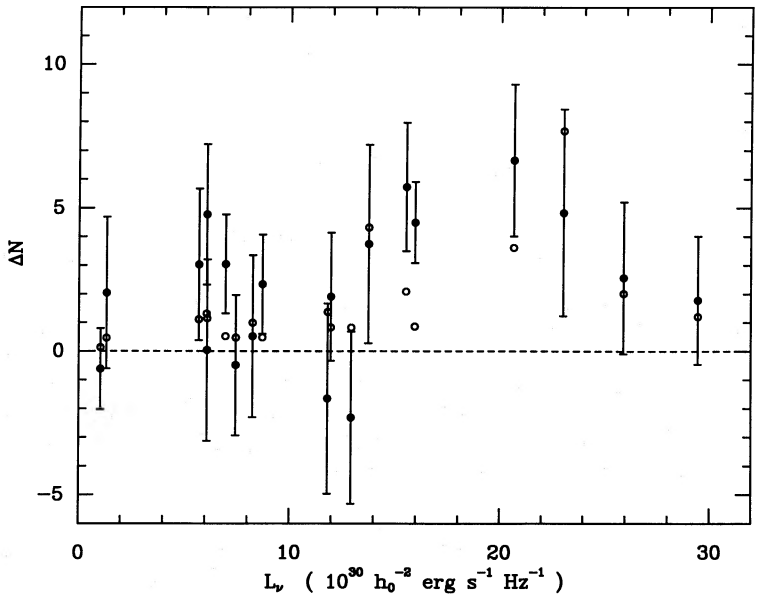

FIG. 1.—Deviation of observed Lyα line number from the cosmological distribution of eq. (1), $\Delta\mathcal{N}$ [eq. (3)], plotted vs. intrinsic Lyman-limit luminosity L_ν [eq. (4)] for each quasar in our sample. The open circles show the predictions of the ionization model [eq. (31)]. Note the trend of increasing line number defect $\Delta\mathcal{N}$ for quasars of higher intrinsic luminosity.

In this equation, $J_\nu(z)$ is the Lyman-limit background radiation intensity (ergs cm^{-2} s^{-1} Hz^{-1} sr^{-1}) at cloud redshift z, and

$$F_\nu^Q = \frac{L_\nu}{4\pi r_L^2} \tag{7}$$

is the local Lyman limit flux density (ergs cm^{-2} s^{-1} Hz^{-1}) due to the QSO. The luminosity distance of the cloud from the QSO is r_L.

Strictly speaking, equation (5) is valid only if the frequency dependence of the background radiation above the Lyman limit is the same as that of the QSO radiation, so that the ratio of ionization rates equals the ratio of Lyman-limit flux densities. This is a good approximation since the background is probably dominated by the radiation from many QSOs.

Equations (5)–(7) describe how the column density of a given Lyα cloud will change near a bright quasar. Since each affected cloud will have a smaller column density of neutral hydrogen N, a larger cloud at the same spot is required to produce a given observed column density. The distribution of observed cloud number in column density has been shown by several groups to be approximated by

$$\frac{d\mathcal{N}}{dN} \propto N^{-\beta} \tag{8}$$

for column densities in the range 5×10^{13} to 5×10^{16} cm^{-2}. Carswell *et al.* (1984) inferred $\beta = 1.68 \pm 0.10$ from the spectrum of QSO 1101−264 ($z \approx 2$). Atwood, Baldwin, and Carswell (1985) found $\beta = 1.89 \pm 0.14$ in the line of sight to QSO 0420−388 ($z \approx 3$). For definiteness we will here assume $\beta = 1.7$, so that the number of clouds above a given threshold N_0 is

$$\mathcal{N}(N \geq N_0) \propto N_0^{-0.7} . \tag{9}$$

Hence for a sample limited by the observed neutral hydrogen column density N, the distribution of clouds with redshift, *including* the quasar proximity effect, is

$$\frac{d\mathcal{N}}{dz} = \mathcal{A}_0(1+z)^\gamma[1+\omega(z)]^{-0.7} , \tag{10}$$

with

$$\omega(z) = \frac{f_\nu}{4\pi J_\nu(z)} \frac{(1+z)^5}{(1+z_Q)} \left[\frac{(1+z_Q)^{1/2}-1}{(1+z_Q)^{1/2}-(1+z)^{1/2}}\right]^2 , \quad \Omega = 1 \tag{11}$$

$$\omega(z) = \frac{f_\nu}{4\pi J_\nu(z)} \frac{4z_Q^2(1+z_Q/2)^2(1+z)^6}{(1+z_Q)[(1+z_Q)^2-(1+z)^2]^2} , \quad \Omega = 0 . \tag{12}$$

Note that the H_0 dependence has cancelled in equations (11) and (12).

a) Cloud Velocity Widths and QSO Proximity

Equation (10) was derived for an N-limited sample; in actuality we use a rest-frame equivalent width limited (W-limited) sample. Hence equation (10) only applies to our data analysis insofar as three idealizations are valid: (1) the N-distribution (8) with $\beta \approx 1.7$ holds for clouds in the *range* of N corresponding to the cutoff W_c and above, (2) column density N and velocity width b are uncorrelated in the cloud distribution, and (3) quasar proximity has no significant effect on b. We now discuss these three idealizations in turn.

1. Assuming a single (unbroken) power-law N-spectrum is tantamount to assuming a single power-law initial mass spectrum, for optically thin clouds. This seems to describe the Lyα forest well. Note that the steepening of the (exponential) W-distribution at low W (MHPB, Fig. 3) is consistent with such a spectrum: the distribution steepens right where clouds become unsaturated for $b \approx 35$ km s^{-1} (Oke and Korycansky 1982; Atwood, Baldwin, and Carswell 1985; MHPB).

2. Some models predict a N-b correlation (Ikeuchi and Ostriker 1986), but there are insufficient data to test this at present. Assuming an uncorrelated distribution is probably a reasonable first approximation in any case.

3. To test whether quasar proximity has an appreciable effect on b, we plot b versus ω for two quasars, Q1101−264 ($z_Q = 2.143$) and Q0420−388 ($z_Q = 3.12$), in Figure 2. These QSOs are the only two for which b values have been estimated for many lines (Carswell *et al.* 1984; Atwood, Baldwin, and Carswell 1985). We counted *all* lines for which measurements of b were available, with no W-cutoff. Hence our line sample in Figure 2 is not complete and may be biased by complex selection effects; however, these selection effects are not likely to vary with ω, which is all we are concerned about here. Average values of b for each ω-bin are shown, with error bars which indicate both the spread in b and intrinsic uncertainties.

Evidently, there is little evidence for variation of b with ω. If there is any trend, it is toward increasing b with increasing ω, but it is not statistically significant. We note in passing that the sense of the apparent trend is in the direction expected on the basis of the ionization model. For larger ω, clouds of a given N are physically larger and would thus have a larger expansion velocity in either pressure-confined or freely expanding cloud models.

Ignoring this complication, we believe that equation (10) provides the best simple physical model for the quasar proximity effect in a W-limited sample.

b) The UV Background

In order to proceed further, we need to estimate $J_\nu(z)$, the background of ionizing photons. Bechtold *et al.* (1987, hereafter BWLM) have done a careful study of this question, based on integrating the UV emission of QSOs in the luminosity function of Schmidt and Green (1983). Heisler and Ostriker (1987, hereafter HO) have also computed $J_\nu(z)$, using a new luminosity function (Heisler and Ostriker 1988), which fits essentially the same data as that of Schmidt and Green plus the gaint quasar survey of Koo and Kron (1988).

For simplicity, in this paper we shall integrate the "pure luminosity evolution" model of Marshall (1985), which is based on a fit to $z < 2.2$ and $B < 20$ quasar data. This has the advantage of being analytic, giving a simple, compact formula for $J_\nu(z)$.

Since the Schmidt-Green and Heisler-Ostriker luminosity functions fit higher z data than those of Marshall, they are apparently more accurate for our purposes. However, this improvement is overshadowed [for the purpose of determining $J_\nu(z)$ at $1.7 < z < 3.8$] by our ignorance of the luminosity function for redshifts greater than ~ 3.4. In any event, we will show that integrations of Marshall's luminosity function, extrapolated to a high z, produce results which are in good agreement with those of BWLM and HO, similarly extrapolated. Thus our analytic results can be regarded as fits to BWLM's or HO's numerical results.

Following Marshall *et al.* (1983), we consider quasars with

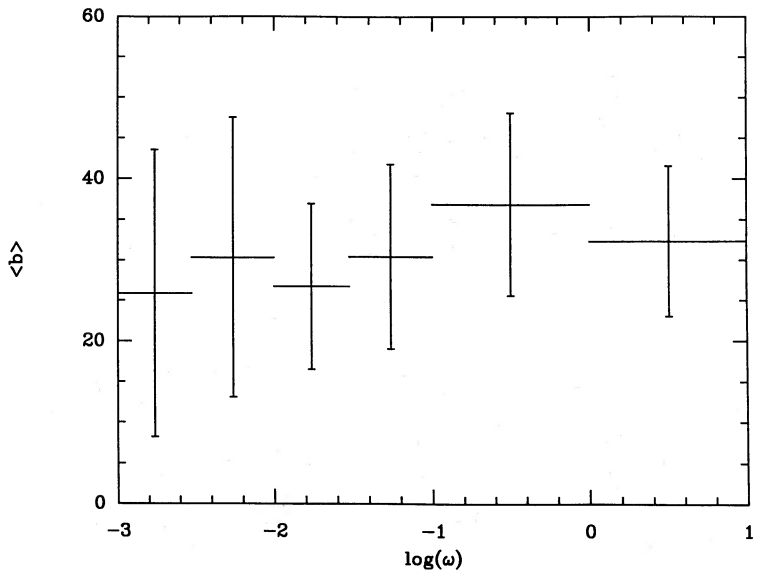

FIG. 2.—Average line velocity-width b (km s^{-1}) vs. flux ratio ω for the quasars Q1101−264 and Q0420−388. In this graph we assume $\Omega = 1$ and $J_\nu(z) = 10^{-21}$ ergs cm^{-2} s^{-1} Hz^{-1} sr^{-1} (a constant). The data are from Atwood, Baldwin, and Carswell (1985) and Carswell *et al.* (1984).
The slight trend shown is in the sense expected in the ionization model, since a larger ω (for a fixed N) corresponds to a physically larger cloud.

intrinsic luminosities evolving like

$$L(z) = \tilde{L} f(z) , \tag{13}$$

where $\tilde{L}$ is the present-epoch luminosity and $f(z)$ is a function of the form $e^{k\tau(z)}$ or $(1 + z)^k$. The present-epoch luminosity function is

$$\rho(\tilde{L}) = \frac{\rho_0}{L_*}\left(\frac{\tilde{L}}{L_*}\right)^{-\alpha_L} . \tag{14}$$

The fiducial luminosity is taken to be $L_* = 10^{30}$ ergs s^{-1} Hz^{-1}. All luminosities in these equations are at a reference equency $\nu_r = (c/2500\ \text{Å})$ in the QSO frame. Thus

$$\rho(z, L) = \frac{\rho_0}{L_*}[f(z)]^{\alpha_L - 1}\left(\frac{L}{L_*}\right)^{-\alpha_L} , \tag{15}$$

with a low-luminosity cutoff at

$$L_{\min} = \tilde{L}_{\min} f(z) . \tag{16}$$

In what follows we use "Model G" from Marshall (1985). This model assumes $\Omega = 1$, intrinsic spectral index $\alpha_0 = -0.5$, and a power-law form for $f(z)$. The resulting fits to the data are

$$\alpha_L = 3.6; \quad f(z) = (1 + z)^{3.2}; \quad \rho_0 = 50 h_0\ \text{Gpc}^{-3};$$
$$\tilde{L}_{\min} = 0.15 L_* .$$

The supply rate of photons of frequency ν is, in general,

$$S_\nu(z) = \frac{L_*}{h\nu}\left(\frac{\nu}{\nu_r}\right)^{\alpha_0}\int_{L_{\min}}^{\infty} dL \rho(z, L)\left(\frac{L}{L_*}\right) . \tag{17}$$

In "Model G,"

$$S_\nu(z) = \frac{13.0\rho_0 L_*}{h\nu_r}\left(\frac{\nu}{\nu_r}\right)^{-0.5}(1 + z)^{3.2} . \tag{18}$$

If all quasars "turn on" at $z = z_{on}$, the integrated background radiation is (Ikeuchi and Ostriker 1986):

$$J_\nu(z) = \frac{c(h\nu)}{4\pi}(1 + z)^{3-\alpha_0}\int_z^{z_{on}} dz \frac{S_\nu(z)}{H(1 + z)^{1-\alpha_0}} . \tag{19}$$

Thus, in the model considered here,

$$J_\nu(z) = j_\nu(1 + z)^{3.5}[(1 + z_{on})^{1.2} - (1 + z)^{1.2}] , \tag{20}$$

where

$$j_\nu = \frac{10.8\rho_0 L_* c}{4\pi H_0}\left(\frac{\nu}{\nu_r}\right)^{-0.5} . \tag{21}$$

Evaluating this at the Lyman limit yields $j_\nu = 8.17 \times 10^{-24}$ ergs cm^{-2} s^{-1} Hz^{-1} sr^{-1}, independent of h_0.

The result is plotted in Figure 3, for $z_{on} = 4$ ("Model I"). Note that if we multiply equation (20) by a factor 0.73, we get two-place agreement with BWLM's integration of Schmidt-Green's HH5 luminosity function across the range $1.8 < z < 3.8$.

We hasten to note that Model I is based upon the assumed existence of quasars at high redshift which have not been found in surveys subsequent to Schmidt and Green. There is evidence that the real distribution of quasars is described by a luminosity dependent cutoff (LDC) at high z, with quasars of higher intrinsic luminosity "turning on" at higher redshifts (Schmidt, Schneider, and Gunn 1986). Following BWLM, we model this by choosing a redshift z_c at which the LDC begins to take force, and evolving the low-luminosity cutoff according to

$$L_{\min} = \tilde{L}_{\min} f(z_c) 10^{\kappa(z - z_c)} \text{ for } z > z_c , \tag{22}$$

with κ and z_c adjustable parameters. We consider two LDC models (see Fig. 3):

$$\text{Model II: } z_c = 2.90; \quad \kappa = 1.0$$
$$\text{Model III: } z_c = 2.75; \quad \kappa = 1.75 .$$

Model III closely resembles the "HH5 LDC, medium intrinsic spectrum" model of BWLM, which is one of BWLM's "best estimates" of the emission of the true observed quasar population.

In summary: Model I resembles the integrated UV emission calculated by BWLM of the Schmidt-Green quasar luminosity function with no high-z cutoff in the QSO number density (until $z = 4$). Hence model I significantly overestimates the UV intensity emitted by the *observed* quasar population for $z > 3$.

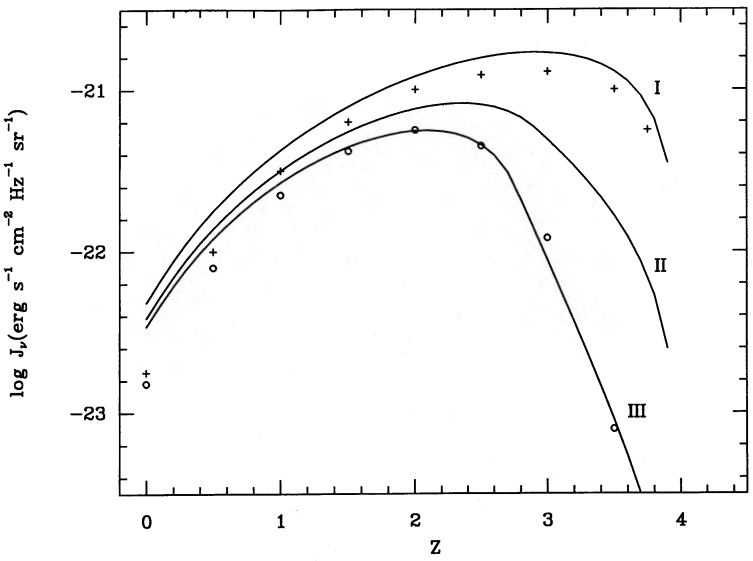

FIG. 3.—Background radiation intensity at the Lyman limit, J_ν, vs. redshift, z, derived from integrations of model QSO luminosity functions. The solid curves, labeled I, II, and III, are derived from pure luminosity evolution models with $\Omega = 1$, a "turn-on" redshift $z_{on} = 4$, and (for II and III) luminosity-dependent cutoffs (LDCs), as described in the text. The crosses (+), put here for comparison with model I, come from Bechtold *et al*'s (1987; BWLM) integration of Schmidt and Green's (1983) model HH5, with "medium" intrinsic spectrum, and no absorption (Figure 3 in BWLM). The circles (○) show BWLM's corresponding LDC model. Heisler and Ostriker's (1987) "Model A," featuring cosmological dust obscuration, is close to model I. Model III is close to BWLM's probable fit to the integrated emissions of observed quasars, assuming no dust.

Note that model I also resembles a background flux model of HO (Model A in Fig. 17 of that paper), which *does* fit the observed high-z quasar population. This model assumes, however, that high-z quasars are appreciably obscured by intervening dust.

Model III represents a best estimate of the integrated UV emission of *observed* quasars according to BWLM (assuming no dust). Model II is an (arbitrary) intermediate case.

IV. COMPARISON OF MODELS WITH OBSERVATIONS

We now determine how well the distribution function (10) describes the data.

a) The General Redshift Distribution

To determine the redshift evolution index γ, we cut off the data sample near each quasar at $\omega_c = 0.1$ and plot log $d\mathcal{N}/dz$ versus log $(1 + z)$ for the remaining data (see Fig. 4). MHPB has also determined γ after deleting data from the vicinity of quasars, using Lyα emission line widths to set the cutoffs. This is not directly related to the zones of enhanced ionization around quasars, however. Our cutoff in ω removes a larger region around quasars which are emitting more ionizing photons.

Since ω depends on J_ν, there is some dependence of our determined γ on the background radiation model. In particu-

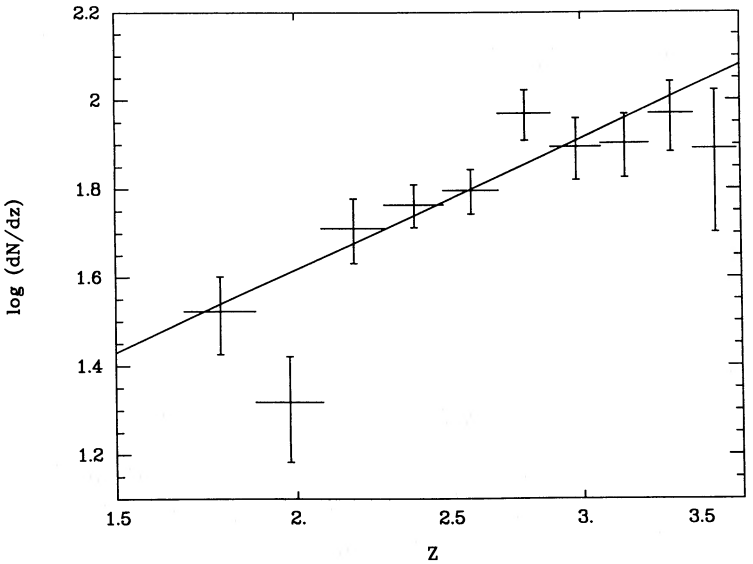

FIG. 4.—Redshift density of observed Lyα lines $d\mathcal{N}/dz$ vs. redshift z for our 19 QSO sample. Although the horizontal axis is labeled in z, intervals of log $(1 + z)$ are equally spaced on the page. The data near each quasar is dropped ($\omega > 0.1$, assuming background flux model I). The rest-frame equivalent width cutoff is 0.36 Å. Fitting parameters are given in the first row of Table 2.

TABLE 2

DETERMINATIONS OF γ

Model	ω_c	γ	$\mathscr{A}_0$	N_{bins}	χ^2	Q	$\mathscr{N}_c$[a]
I	0.1	2.36 ± 0.42	3.07	10	12.6	0.13	416
II	0.1	2.7 ± 0.5	1.96	10	13.4	0.10	367
III	0.1	3.22 ± 0.6	1.16	10	12.2	0.14	298
I	0.1	2.33 ± 0.40	3.20	18	16.8	0.47	416
I	∞	2.13 ± 0.35	3.88	10	11.7	0.17	470
I × 10	0.1	2.4 ± 0.4	2.85	10	11.7	0.16	461

[a] The total number of lines counted.

lar, the ω-cutoff significantly reduces the amount of high-z data when LDC models of $J_\nu(z)$ are used, and this apparently increases the estimate of γ in our data sample, with a concurrent increase in the uncertainty (cf. the first three rows of Table 2).

A more accurate way to determine γ might be to use the "proximity-corrected redshift interval,"

$$Y \equiv \int [1 + \omega(z)]^{-0.7} dz , \tag{23}$$

and examine the z-distribution of $d\mathscr{N}/dY$. This depends on equation (10) being correct, however, which is not yet established, so we adopt a simple cutoff in ω here.

Although the data analysis we use here relies on binning, we have checked that our results are only weakly sensitive to the choice of bins. In Table 2 we give two determinations of γ for background model I, one based on binning the redshift range of the data into 10 equal bins, and one for 18 equal bins (rows 1 and 4 in the table). There is evidently good agreement between the two cases, and reasonable values of the χ^2 probability function Q are obtained in all cases. (Note: no uncertainty is quotted for $\mathscr{A}_0$ in Table 2 because $\mathscr{A}_0$ is strongly correlated with γ.)

Our value of $\gamma = 2.36 \pm 0.40$ is in reasonable agreement, although slightly larger, than most recent determinations in the literature (MHPB). This is to be expected, since if the proximity effect is ignored, γ is (incorrectly) found to be systematically smaller (cf. row 5 of Table 2), as MHPB have noted.

We call attention to the deviant point near $z = 2$ in Figure 4. As far as we have been able to determine this is just a statistical anomaly, not an indicator of any failure to model the data properly.

b) The Distribution in ω

In terms of the "coevolving redshift interval," defined as

$$X_\gamma \equiv \int (1 + z)^\gamma dz , \tag{24}$$

equation (10) becomes

$$\frac{d\mathscr{N}}{dX_\gamma} = \mathscr{A}_0(1 + \omega)^{-0.7} . \tag{25}$$

Using $d\mathscr{N}/dX_\gamma$ rather than $d\mathscr{N}/dz$ removes the basic trend in the data and allows us to concentrate on the proximity effect.

In Figure 5 we plot $d\mathscr{N}/dX_\gamma$ versus log ω for our data sample, assuming background flux model I. We find good agreement with equation (25). Since this one of our most important figures, we give some details of how it was made.

We divided the interval $-4 < \log \omega < -1$ into four equal bins. The region $\log \omega > -1$, with a lower density of lines, is divided in three at $\log \omega = 0$ and 1 (see Table 3). Note that the horizontal bar for the rightmost bin technically should extend to infinity, since we *could* detect narrow absorption lines right up to the peak of Lyα emission. Our actual largest ω line, however, lies at $\omega \approx 50$. This is where the vertical bar is positioned on the graph.

Having set the bin boundaries in ω, we solve equation (11) for $z^b(j, k)$ and $z(j, k)$, the biggest and smallest values of z for

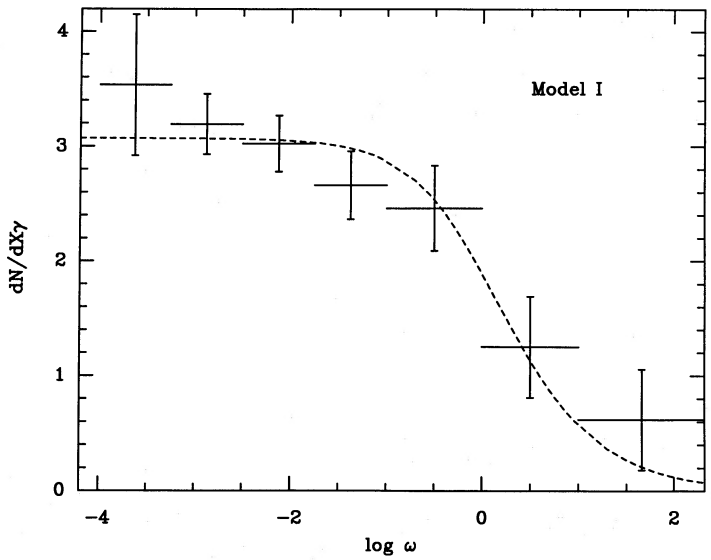

FIG. 5.—Density of observed Lyα lines in "coevolving redshift" [eq. (24)], $d\mathscr{N}/dX_\gamma$, plotted vs log ω, the logarithm of the Lyman-limit flux density ratio (QSO flux/background) (eqs. [6] and [11]), for background flux model I [eqs. (20)–(21) and Fig. 3]. The dashed line is the prediction of the ionization model, eq. (25). Data points are listed in Table 3.

The "coevolving redshift interval" X_γ is defined so that the general (cosmological) trend in the line number density [eq. (1)] is suppressed in this figure, extricating the proximity effect for study. The drop-off of line density with increasing ω apparently traces the enhanced ionization of Lyα clouds near bright quasars.

An earlier version of this figure appearing in Princeton University Observatory Preprint, No. 225, 1987 differed only in the choice of bin boundaries from the version printed here. It showed a more pronounced flattening at $\log(\omega) < -2$.

TABLE 3

BINNED DATA FOR FIGURE 5

Bin (j)	$\log \omega_{min}$	$\log \omega_{max}$	$\Delta X_{\gamma j}$	$\mathcal{N}_j$	$(d\mathcal{N}/dX_\gamma)_j$
1.....	−4.00	−3.25	9.333	33	3.536
2.....	−3.25	−2.50	46.36	148	3.193
3.....	−2.50	−1.75	50.94	154	3.023
4.....	−1.75	−1.00	30.43	81	2.662
5.....	−1.00	0.00	17.88	44	2.461
6.....	0.00	1.00	6.399	8	1.250
7.....	1.00	∞	3.230	2	0.619

bin j of quasar k. The total number of lines and the total X_γ in bin j are then found by

$$\mathcal{N}_j = \sum_k \mathcal{N}_{j,k} \quad \text{and} \quad \Delta X_{\gamma j} = \sum_k \int_{z^s(j,k)}^{z^b(j,k)} (1+z)^\gamma \, dz \, . \quad (26)$$

These quantities are tabulated in Table 3. Their ratio is $d\mathcal{N}/dX_\gamma$. The 1-σ error bars in Figure 5 are simply this ratio divided by $(N_j)^{1/2}$. (Of course, if either $z_{L,k}$ or one of the excluded regions noted in Table 1 lie in bin j, the formula for $\Delta X_{\gamma j}$ must be adjusted.)

Note that if we had used BWLM's integration of Schmidt-Green's HH5 model (with no absorption and "medium" intrinsic spectrum; see Fig. 3), all data points in Figure 5 would shift an amount

$$\Delta \log \omega = -\log (0.73) = 0.14$$

to the right, which is not a significant change.

We constructed graphs like Figure 5 for several alternative background flux models (Fig. 6). The χ^2 probability function Q for each graph is given in Table 4.

To show that the poor fit obtained for model II in Figure 6*a* is *not* due to the fact that γ is larger in model II than in model I, we made Figure 6*c* with $\gamma = 2.36$. In Figure 6*b* (flux model III), $\Delta X_{\gamma j} = 0$ in the leftmost bin ($-4 < \log \omega < -3.25$) so this bin was dropped. Figure 6*d* assumes a background radiation intensity 10 times larger than model I at every redshift, which we call "model I × 10".

Apparently, we can exclude models II, III, and I × 10 in favor or model I with high confidence. We will discuss the implications of this in § VI.

It is important to extend the ω-range of the $d\mathcal{N}/dX_\gamma$ versus ω graph to the lowest values possible, as we have done in Figures 5 and 6. Although ideally one expects no change in $d\mathcal{N}/dX_\gamma$ for $\log(\omega) < -1.5$, if the assumed background flux is not correct, such variations can be produced. Moreover, even if we knew $J_\nu(z)$ with high confidence, it would be useful to extend the graph to small ω as a consistency check of the theoretical picture given here. The theory is tenable as long as $d\mathcal{N}/dX_\gamma$ levels off in ω to within statistical uncertainty at very small ω. For more on this subject, see § V.

TABLE 4

$d\mathcal{N}/dX_\gamma$ VERSUS ω FITS

Model	γ	$\mathcal{A}_0$	N_{bins}	χ^2	Q	Figure
I	2.36	3.07	7	2.99	0.89	5
II	2.74	1.96	7	19.07	0.008	6*a*
III	3.20	1.16	6	38.38	1×10^{-6}	6*b*
II	2.36	3.07	7	18.04	0.01	6*c*
I × 10	2.40	2.85	7	18.77	0.009	6*d*

In summary, Figure 5 presents the basic result of this paper. *The decline in the number of Lyα line systems seen in the vicinity of quasars (crosses) is well fitted by a simple physical model (dashed line) based on the ideal that each quasar, by its extra ionizing radiation, reduces the neutral hydrogen content of nearby clouds.*

c) *Correlation with Intrinsic Luminosity*

Figure 1 demonstrates a positive correlation between quasar intrinsic luminosity and deviations from the general redshift distribution, equation (1). Does this correlation agree in detail with the ionization model?

To answer this question we study the line distribution within a luminosity distance $r_L = 8$ Mpc of each quasar. This corresponds to

$$\omega \geq 0.010 L_{30} J_{21}{}^{-1} \, , \quad (27)$$

where L_{30} is L_ν in units 10^{30} cgs, and J_{21} is J_ν in units 10^{-21} cgs. The redshift cutoff corresponding to $r_L = 8$ Mpc is (approximately, for $\Omega = 1$)

$$z_R = z_Q - 0.0027 h_0 (1+z_Q)^{5/2} \, . \quad (28)$$

The expected number of lines, in the cosmological distribution with *no* proximity effect, is

$$\mathcal{N}_\gamma = A_0 \int_{z_R}^{z_Q} (1+z)^\gamma \, dz \, . \quad (29)$$

Including the effect of quasar ionization, the expected number is

$$\mathcal{N}_i = A_0 \int_{z_R}^{z_Q} (1+z)^\gamma [1 + \omega(z)]^{-0.7} \, dz \, . \quad (30)$$

We write $\mathcal{N}_0$ for the *observed* line number in the inerval (z_R, z_Q). These numbers are given for each QSO in Table 5. (We assume flux model I.)

The expected deviation from the cosmological distribution, in the ionization model, is

$$\Delta \mathcal{N}_{exp} = N_\gamma - N_i \, . \quad (31)$$

TABLE 5

LYα LINE NUMBERS FOR $r_L \leq 8$ MEGAPARSECS[a]

z_Q	L_ν[b]	z-Class	L_ν Class	$\mathcal{N}_\gamma$	$\mathcal{N}_0$	$\mathcal{N}_i$
1.725.....	1.04	1	1	1.38	2	1.25
1.899.....	8.71	1	2	1.71	0	1.27
1.937.....	7.45	1	2	1.82	1	1.38
2.051.....	6.96	1	2	2.16	2	1.67
2.143.....	15.93	2	3	2.47	1	1.70
2.181.....	12.94	2	3	2.61	3	1.87
2.200.....	29.45	2	4	2.69	1	1.63
2.223.....	11.97	2	3	2.77	2	2.01
2.518.....	8.25	3	2	4.14	5	3.20
2.605.....	1.32	3	1	4.63	6	4.18
2.656.....	11.81	3	3	4.94	7	3.65
2.690.....	25.91	3	4	5.15	2	3.31
2.763.....	5.70	4	2	5.64	2	4.57
2.765.....	6.09	4	2	5.65	5	4.55
2.877.....	6.06	4	2	6.47	3	5.21
3.120.....	15.51	5	3	6.82	3	4.86
3.280.....	20.64	5	4	10.19	4	6.73
3.540.....	13.75	5	3	13.38	10	9.16
3.786.....	23.04	5	4	17.02	12	9.42

[a] For $\Omega = 1$ and $H_0 = 100$ km s^{-1} Mpc^{-1}.
[b] In units 10^{30} ergs s^{-1} Hz^{-1}.

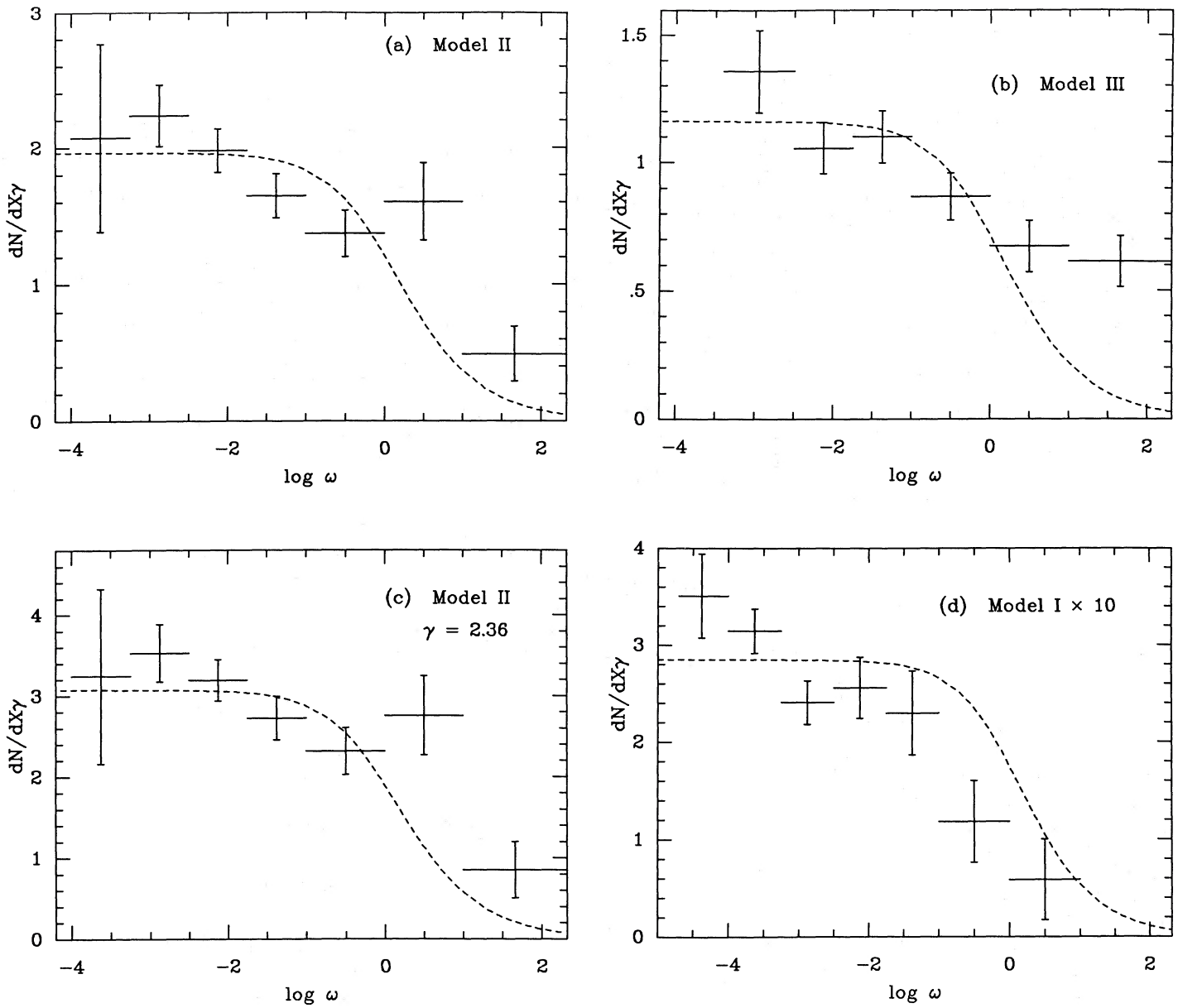

FIG. 6.—Density of observed Lyα lines in "coevolving redshift" (eq. [24]), $d\mathcal{N}/dX_\gamma$, plotted vs. log ω, the logarithm of the Lyman-limit flux density ratio (QSO flux/background) [eqs. (6) and (11)], for four alternative background flux models $J_\nu(z)$. The dashed line shows the prediction of the ionization theory for each background flux model (eq. [25]). These graphs differ from Fig. 5 only in the assumed $J_\nu(z)$ models, which are described in § III*b* and plotted in Fig. 3. Input parameters for each graph are given in the last four rows of Table 4. Fig. 6*d* ("I × 10") assumes a background radiation intensity 10 times larger than Model I at every redshift.

Apparently, all four models shown here afford significantly worse fits to the theory than the model of Fig. 5. This is quantified in Table 4, where χ^2 probability functions Q are given for each model. We conclude that background flux model I is closer to the true background flux than all other J_ν models considered.

This is plotted for each quasar as an open circle in Figure 1. (For this figure, $z_R \rightarrow z_Q - \Delta z$ in eqs. [29]–[30].) Note that the total number of "missing lines" due to the proximity effect is only $\sum_i \Delta\mathcal{N}_{\rm exp} \approx 35$ out of ~ 470 for our 19 quasar sample complete to $W = 0.36$ Å (rest frame). But the underdensity is concentrated near each QSO in a well-defined way, so it is not lost in statistical noise. The fact that the open circles in Figure 1 typically lie along the error bars is evidence for the correctness of the model.

In order to quantify how the proximity effect correlates with L_ν, we divide the quasars into four "luminosity classes," taking advantage of the natural groupings in L_ν which are apparent in Figure 1 (see Table 5). Total values of $\mathcal{N}_0$, $\mathcal{N}_\gamma$, and $\mathcal{N}_i$ are found for each L_ν class by summing the individual quasar values. The fractional deviation of line number from the cosmological distribution in each class is then

$$\Lambda_\gamma = \frac{\mathcal{N}_\gamma - \mathcal{N}_0}{\mathcal{N}_\gamma} . \tag{32}$$

The fractional deviation from the ionization model distribution is

$$\Lambda_i = \frac{\mathcal{N}_i - \mathcal{N}_0}{\mathcal{N}_i} . \tag{33}$$

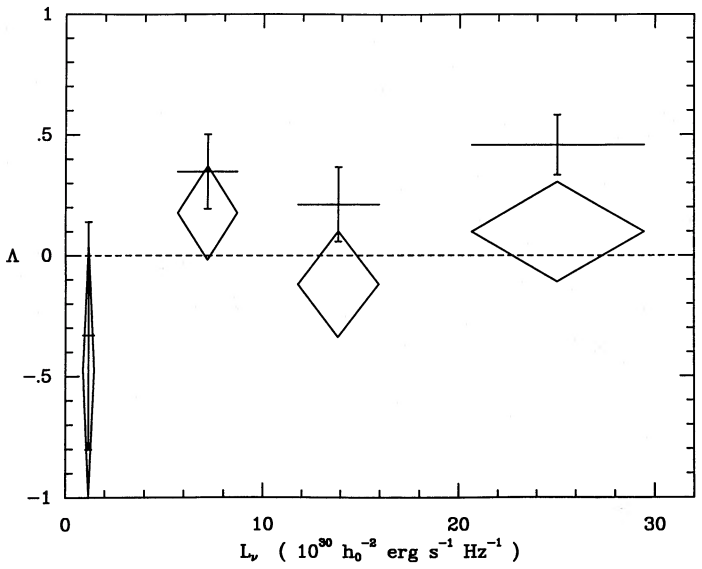

FIG. 7

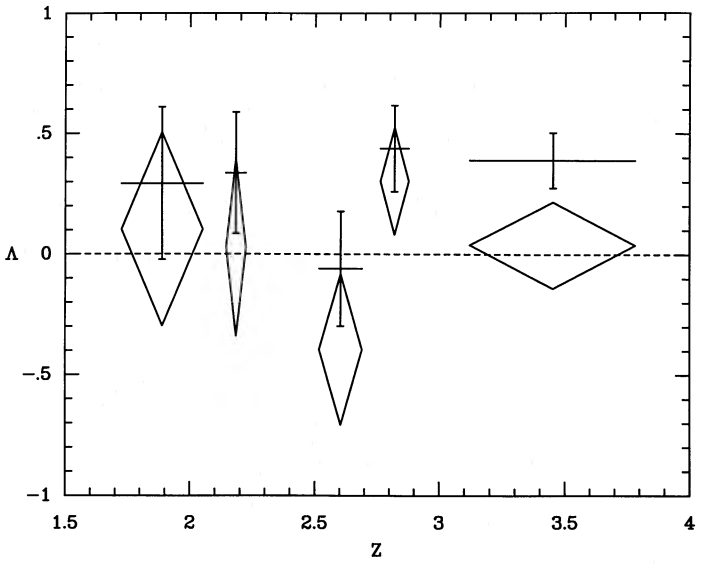

FIG. 8

FIG. 7.—Fractional line number deviations Λ vs. intrinsic Lyman-limit quasar luminosity L_ν (eq. [4]) for four quasar luminosity classes. The crosses denote Λ_γ, the fractional deviation from the general (cosmological distributions (eqs. [32] and [29]). The triangles denote Λ_i, the fractional deviation from the ionization model distribution (eqs. [33] and [30]), assuming background flux model I. Deviations are calculated for $r_L \leq 8.0$ Mpc in the spectrum of each quasar, assuming $\Omega = 1$ and $H_0 = 100$ km s^{-1} Mpc^{-1} (see Table 5). Vertical error bars are given by eq. (34); horizontal error bars measure the width of each L_ν class. The meaning of this figure is described in the paragraph following equation (34) in the text.

FIG. 8.—Fractional line number deiations Λ_γ, Λ_i [eqs. [32]–[33]) vs. redshift z for five quasar redshift classes. Symbols have the same meaning as in Fig. 7. For an interpretation of this figure, see the concluding three paragraphs of § IV*c*.

These quantities are plotted in Figure 7, with error bars

$$\delta\Lambda_\gamma = \frac{(\mathcal{N}_0)^{1/2}}{\mathcal{N}_\gamma}\,,\quad \delta\Lambda_i = \frac{(\mathcal{N}_0)^{1/2}}{\mathcal{N}_i}\,. \tag{34}$$

What does Figure 7 tell us? First of all, the very fact that the Λ_γ points (crosses) lie generally above the horizontal axis indicates that there is a proximity effect. Insofar as Λ_γ increases with increasing L_ν, there is a positive correlation of the proximity effect with intrinsic QSO luminosity. It is only a 1 σ trend here. The fact that the Λ_i points (triangles) lie on the horizontal axis to within statistical uncertainty, and show no overall rising or falling trend, indicates that the ionization model fits the data tolerably well. Note that the crosses and triangles are increasingly displaced from each other with increasing L_ν.

Figure 8 is a similar graph for redshift classes. Any strong trend in the position of the triangles in this graph might tell us, for example, that we have the z-dependence of J_ν wrong. This figure is noisier than Figure 7 because we have divided the data into smaller groups (five z-classes), but the ionization model again fits reasonably well.

As noted earlier, there exists a weak positive correlation of L_ν with z_Q in our quasar sample (correlation coefficient $\xi = 0.354$). Because of this, one might suspect that any observed correlation of Λ_γ with L_ν (Fig. 7) is simply an artifact of a strong correlation of Λ_γ with z. Figure 8 argues against such an interpretation since there is no strong trend of Λ_γ with z. The fractional line number defect Λ_γ is not strongly correlated with z, even though the absolute line number defect $\Delta\mathcal{N} = \Lambda_\gamma \mathcal{N}_\gamma$ is correlated. This lends support to the ionization model.

Our assertions are obviously not confirmed with high statistical confidence given the existing data set, but can be proved or disproved using these methods when more data are available.

d) Angular Range of the Proximity Effect

If a quasar emits isotropically (rather than towards the observer) it will deplete the Lyα cloud population in a spherical zone around it, and lines of sight to *other* quasars which pass through this zone should show the depletion. This test of the ionization model was pointed out to us by B. Paczyński (1987). We now calculate the angular distance on the sky around a quasar (of Lyman-limit flux density f_ν and redshift z_Q) where enhanced ionization of the Lyα forest should be observable.

Specifically, consider the surface in space defined by $\omega = 0.1$. Equation (11) gives the redshift z along our line of sight at which $\omega = 0.1$, for given values of f_ν, z_Q, and $J_\nu(z)$. The luminosity distance of the cloud from the QSO is

$$r_L = \frac{2c}{H_0}\,\frac{(1+z_Q)^{1/2} - (1+z)^{1/2}}{(1+z_Q)(1+z)}\,. \tag{35}$$

This is related to the cosmological scale parameter $R(z)$ and the Robertson-Walker coordinate distance Δx by

$$r_L = \left(\frac{1+z_Q}{1+z}\right) R(z)\,\Delta x\,. \tag{36}$$

The *proper* distance r_p at $z = z_Q$ for $\omega = 0.1$ is

$$r_p = R(z_Q)\,\Delta x = \left(\frac{1+z}{1+z_Q}\right)^2 r_L\,. \tag{37}$$

The angular size on the sky is (Peebles 1971)

$$\theta = \frac{H_0\, r_p (1+z_Q)^{3/2}}{2c[(1+z_Q)^{1/2} - 1]}\,, \tag{38}$$

which implies

$$\theta = \left[\frac{(1+z_Q)^{1/2} - (1+z)^{1/2}}{1 + z_Q - (1+z_Q)^{1/2}}\right]\frac{1+z}{1+z_Q}\,. \tag{39}$$

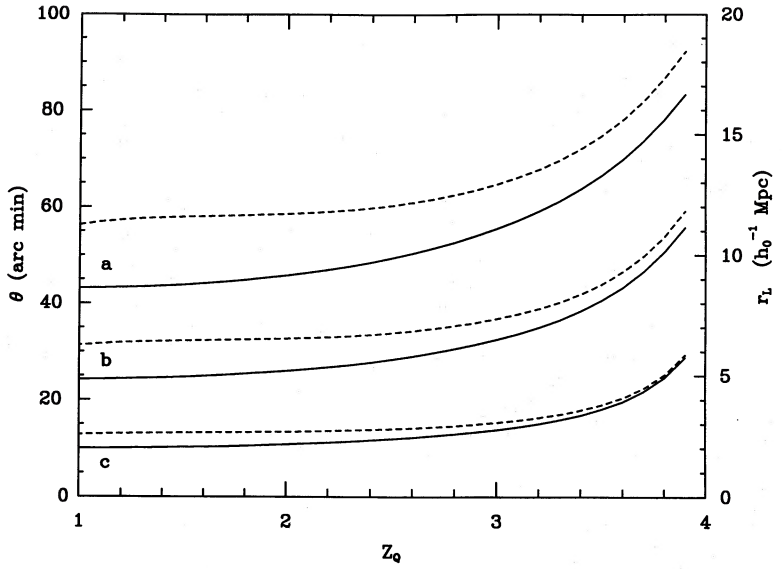

FIG. 9.—Angular extent θ on the sky (*solid lines, left scale*) and local luminosity radius r_L (*dashed lines, right scale*) of zones of enhanced ionization ($\omega \geq 0.1$) around quasars, plotted vs. quasar redshift z_Q (eqs. [39] and [35], with z given by eq. [11] where $\omega = 0.1$). Curves *a*, *b*, and *c* refer to different values of the observed Lyman-limit flux densities f_ν: *a*, 11.0; *b*, 3.4; *c*, 0.57 in units 10^{27} ergs cm^{-12} s^{-1} Hz^{-1}. These correspond to the largest and smallest f_ν value in our sample (and an intermediate value), with apparent QSO magnitudes m_v: *a*, 15.9; *b*, 16.9; and *c*, 19.0.

This is plotted in Figure 9, for the range of f_ν in our sample. Note that the angle is of order 1° for the more luminous quasars.

e) Gravitationally Lensed QSOs and the Proximity Effect

It is interesting to note that since gravitationally lensed quasars are not as bright as they appear to be they should show a correspondingly small proximity effect, thus providing a test for both the lensing hypothesis and our interpretation of the proximity effect.

The one lensed quasar in our sample, Q1115+080 at $z_Q = 1.725$, is amplified by a factor of 8.7 (Young *et al.* 1981). The expected number of lines for $r_L < 8$ Mpc is $\mathcal{N}_i = 1.25$ (eq. [30] and Table 5). Without gravitational lens amplification taken into account, the expected number would be 1.02. The observed number is $\mathcal{N}_0 = 2$, which gives very slight corroboration of the lensing hypothesis.Of course, a much stronger test could be made using many high-z lensed quasars.

f) BL Lac objects and the Proximity Effect

In the standard model for BL Lac objects, the objects emit radiation beamed directly at the observer (Blandford and Königl 1979). Hence BL Lac objects should *not* give rise to enhanced ionization in the line of sight to more distant objects that lie nearby on the sky, although they *should* deplete the Lyα clouds in their own line of sight. This is a potentially important test, since it could offer direct confirmation of the beaming hypothesis.

Incidentally, if some BL Lac objects are microlensed OVV quasars as suggested by Ostriker and Vietri (1986), the proximity effect should be small in *all* directions for these objeects, as mentioned above. We will say more about BL Lac objects and OVV quasars when we discuss quasar variability in § V.

V. QUASAR LUMINOSITY VARIATIONS: THE "ANOMALY"

D. Tytler (1987) did a study of the proximity effect based on essentially the same data set as ours. He binned line number data in rest-frame absorption wavelength,

$$\lambda_r = \left(\frac{1+z}{1+z_Q}\right)1216 \text{ Å}$$

(his Fig. 2). He found evidence that the "inverse effect" in the data is real, but that it extends farther from the QSO than would be expected for the effect of quasar ionization. He called the trend of increasing line density far from the quasar "the anomaly" and concluded that it is probably a spurious effect, due to line blending. He also noted that there exists a statistically significant underdensity of lines very close to quasars which may be due to enhanced ionization, but he did not quantitatively compare this with the expectations of an ionization model.

When we compare the data with a detailed model, we find that the ionization effect is clearly present as predicted, but we find only weak evidence that there exists an anomaly as defined by Tytler. Our use of the flux ratio variable ω rather than λ_r probably accounts (at least in part) for this different conclusion. Since L_ν varies over a factor of ~ 30 in the QSO sample, this is an important refinement.

The gradual rise of the data points with decreasing $\omega < 0.1$ in Figure 5, where the model predicts a nearly constant value of $d\mathcal{N}/dX_\gamma$, constitutes our (weak) evidence for "the anomaly." This trend is within statistical uncertainty in the present study ($Q = 0.89$ for model I). But if it is found to be statistically significant in future analyses based on larger data samples, it is not *necessarily* a sign of inhomogeneities in the data sample.

There is an alternative explanation for deviations from our model that we must explore. Namely, intrinsic luminosities of quasars probably vary on time scales short compared to equilibriation times in the Lyα clouds (or on comparable time scales). The equilibriation time is

$$\tau \equiv n_{\rm H\,I}\left(\frac{dn_{\rm H\,I}}{dt}\right)^{-1}, \qquad (40)$$

which, under the relevant physical conditions, is (Black 1981):

$$\tau = 1 \times 10^4 (1+\omega)^{-1} J_{21}{}^{-1} \text{ yr} . \quad (41)$$

We have little reliable data on QSO luminosity changes on this time scale, but it is plausible that such luminosity changes appreciably "smooth out" the proximate cloud distribution (eq. [25]). In order to demonstrate this in a general way, we consider the following simple model:

Imagine that quasar magnitudes vary randomly across a range $\sim\sigma$. In particular, the *observed* magnitude M_0 is drawn from a Gaussian distribution of width σ. The effective ionizing magnitude at the cloud, M_i, which is the magnitude at which the cloud *would* be in equilibrium, is drawn from the same distribution. We measure M_0, and assume that we know σ. The probability distribution for M_i is then

$$P(M_i) = \frac{1}{2(\pi)^{1/2}\sigma} \exp\left[\frac{-(M_i - M_0)^2}{4\sigma^2}\right] . \quad (42)$$

Equation (25), adjusted to take such quasar luminosity variations into account, is

$$\frac{d\mathcal{N}}{dX_\gamma} = \frac{A_0}{2\sigma(\pi)^2} \int_{-\infty}^{\infty} e^{-(y^2/4\sigma^2)} (1 + \omega \times 10^{-0.4y})^{-0.7} dy . \quad (43)$$

This is plotted in Figure 10. Note that a magnitude variation $\sigma \approx 2.5$ (a factor of ~ 10 in L_ν) might account for the "anomaly" of Figure 5. In other words, the fact that a proximate distribution (eq. [10]) convolved with a $\sigma = 2.5$ Gaussian fits observations better than the unconvolved distribution may indicate that quasar magnitudes vary by ~ 2.5 on time scales $\sim 10^4$ yr or less. Note that since we are allowing QSO luminosities to fluctuate to *lower* values than observed as well as higher, we can account for the overdensity of lines (compared to the ionization model) in the rightmost bin of Figure 5 as well. There is indeed a 1 σ overdensity in this bin, since the expected number of lines is $\mathcal{N}_i = 0.80$ [from eq. (30), with $z_R \rightarrow z_i(\omega = 10)$, summed over 19 quasars] and we observe $\mathcal{N}_0 = 2$. With no proximity effect, the expected number would be $\mathcal{N}_\gamma = 9.92$.

Optically violent variable (OVV) quasars should show a very "smoothed" proximate cloud distribution, if a group of these objects were used to construct a graph like Figure 5. BL Lac objects, on the other hand, should show an anomalously weak proximity effect, since these objects are probably observed only in a transient state of high luminosity.

Note that the four largest L_ν quasars in our sample show anomalously strong depletion of Lyα clouds at $\omega < 0.1$. This is evident from Figure 11, where we plot Λ_γ and Λ_i with *no z-cutoff*; i.e., the lower limits of the integrals in equations (29) and (30) are taken at z_L. This might indicate that the highest L_ν quasars in our sample were brighter in the past and are now rapidly evolving to lower luminosities.

VI. CONCLUSIONS

a) *Quasar Ionization of Lyα Clouds*

We have shown that "inverse effect" in the Lyα cloud distribution can be attributed to the enhanced ionization of clouds near the quasars in whose spectra they are observed. The regions affected are typically large: 20′ or 5 Mpc.

It might be possible to find other explanations, not based on cloud ionization, for the observed phenomena. For example, QSOs might be spatially correlated with regions of high-pressure intergalactic gas, which reduce cloud sizes and render clouds less detectable. But it would be difficult to explain the correlation between the underdensity of lines and intrinsic quasar luminosity in such a model (Figs. 1 and 7).

b) *The Cosmological Cloud Distribution*

The redshift evolution index for Lyα clouds, γ, is found to be systematically larger when the quasar proximity effect is taken into account. For our sample of 19 QSOs complete to rest frame equivalent width 0.36 Å, we find $\gamma = 2.36 \pm 0.40$ in the

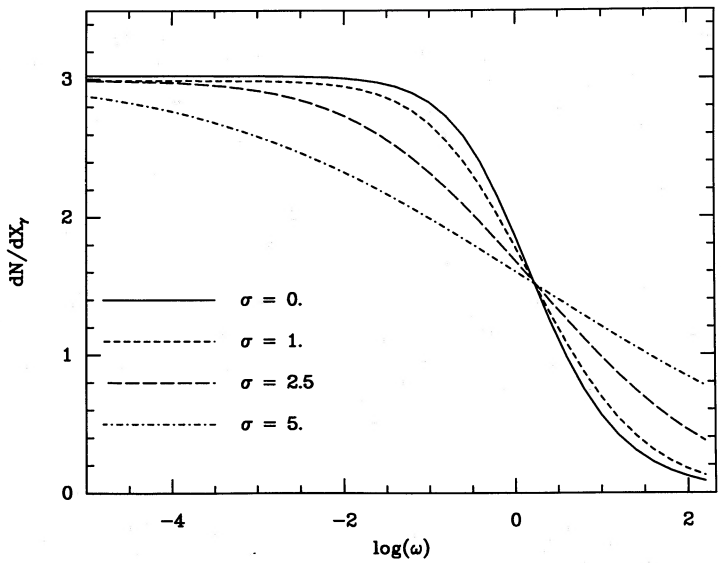

FIG. 10.—Line density in "coevolving redshift" $d\mathcal{N}/dX_\gamma$ vs. flux ratio ω, for cloud ionization models, including the effects of quasar time variability in a statistical way (eq. [43]). The standard deviation of QSO magnitudes due to stochastic variability is σ. Note that a curve lying between the small-dashed and large-dashed curves ($1 < \sigma < 2.5$) would fit the data in Fig. 5 better than the $\sigma = 0$ curve. This might be evidence for quasar variability at the $\sigma \approx 2$ level on timescales $\sim 10^4$ [eq. (41)].

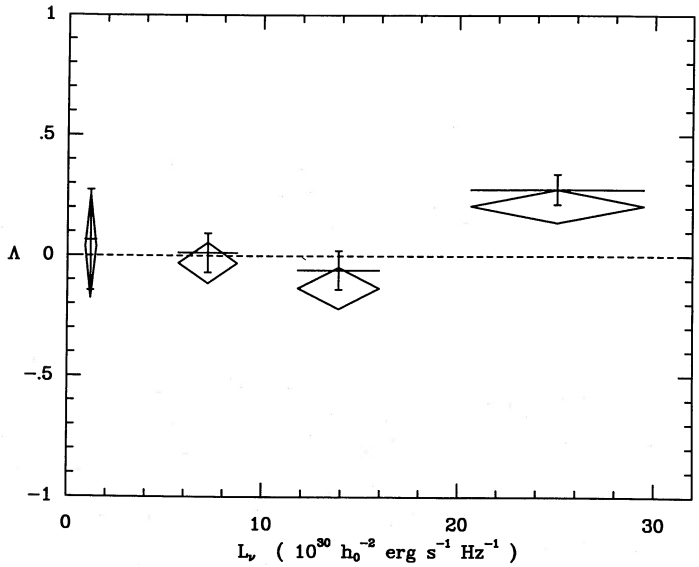

FIG. 11.—Fractional line number deviations Λ_γ, Λ_i (eqs. [32]–[33]) vs. intrinsic QSO luminosity L_ν [eq. (4)] for four quasar luminosity classes, with redshift lower bounds in each quasar spectrum at z_L (Table 1). Instead of concentrating on the line number deviation in a narrow zone near each quasar, here we plot the fractional deviation in the entire spectral region where we have a complete, uncontaminated line sample, Symbols have the same meaning as in Fig. 7. Background flux model I is assumed. Although the proximity effect is generally lost in statistical noise in this figure, the highest L_ν class apparently shows an anomalously large line defect. This might indicate that the four QSOs in this class were brighter in the past, due to stochastic time variations or to a secular decline in luminosity.

relation $d\mathcal{N}/dz = \mathcal{A}_0(1+z)^\gamma$. Ignoring the proximity effect, we find (incorrectly) $\gamma = 2.13 \pm 0.35$.

c) *The UV Background*

If the ionization model is correct, the distribution of clouds near quasars can be used to infer the UV background at large redshift. This represents the first physical "measurement" of the high-z ionizing background: all previous determinations have been inductive, based on integrating the radiation of known UV emitters. Our present data imply, roughly speaking, that the background radiation is constant for $1.7 < z < 3.8$ and given by

$$\log J_\nu = -21.0 \pm 0.5 ,$$

where J_ν is the Lyman limit intensity (ergs cm^{-2} s^{-1} Hz^{-1} sr^{-1}). Much more data will be required to make this determination firm. Nevertheless, we can rule out background flux models based on integrating the UV emissions of quasars with a luminosity-dependent cutoff at $z > 2.7$ (our models II and III) with a high level of confidence (see Table 4).

P. Shapiro (1984) showed that observed quasars are not numerous and luminous enough to photoionize the IGM (assuming $\Omega h^2 \approx 0.01$–0.1) before $z \approx 3$ in order to satisfy the Gunn-Peterson test. Our analysis indicates that the background of ionizing photons at $z \geq 3.5$ is *already* high, which is consistent with Shapiro's result, although it is not clear where this UV radiation is coming from. There are two possibilities;

1. There exist sources of ionizing radiation at $z > 3$ besides QSOs which are comparable, in integrated photon number, to the extrapolated (no LDC) quasar population; or

2. the observed drop-off of the QSO number density for $z \geq 2.5$ is not real and many high-z QSOs are obscured by dust.

Possible alternative sources of ionizing photons include young elliptical galaxies (BWLM) or "Population III" pregalactic stars (Carr, Bond and Arnett 1984), although we have no direct observations of these objects at $z \geq 3$.

The role of dust in this context needs further investigation. To model the UV background in a universe with significant obscuration, one must take into account both the increased number and luminosity of sources, and the increased absorption (Ostriker and Heisler 1984; HO). Model I, our best-fit model, does agree well with Model A of HO (see Fig. 17 in that paper) which includes both dust and a quasar population not cut off at $z = 3$.

d) *Evidence for Quasar Luminosity Variations*

The four most luminous quasars in our sample (at redshifts 2.20, 2.69, 3.28, and 3.78) apparently affect their environment more strongly than one would expect from their observed luminosities (Fig. 11). In particular, the fact that the fourth bin in Figure 5 lies more than 1 σ below the model prediction can be entirely attributed to these four quasars. This may indicate that these very luminous quasars have been brighter in the past and are now diminishing in luminosity on time scales short compared to equilibration times in the Lyα clouds. This might be due to either stochastic variations or to a secular decline in luminosity.

It has been suggested that line blending is partly responsible for the "inverse effect" in the observed line distribution. Scanning blueward through a spectrum, instrumental throughput and detector sensitivities decline, causing a systematic decrease in signal-to-noise ratio. Weak Lyα lines that are individually below the equivalent-width cutoff could (conceivably) be increasingly blended to form spurious strong lines (Tytler 1987).

We find no evidence that this is a significant effect in the spectra we studied, with $W_c = 0.36$ Å. If, however, it were present at low levels, it would be difficult to extricate from the effects of intrinsic QSO luminosity variations (Fig. 10). Analysis of Monte Carlo–simulated spectra may help (Jenkins 1988). In some instances, line blending could affect spectra in a sense opposite to the "inverse effect"; i.e., two close but distinct lines, both above the cutoff, could be counted as one.

e) *Further Tests*

i) *Improved Statistics*

With a larger, more homogeneous, statistically complete catalog of QSO absorption lines, the proximity effect analysis could be profitably done using nonparametric statistics (maximum likelihood method, Kolmogorov-Smirnoff test). A more systematic determination of background UV flux would then be possible. Deviations from the simple, power-law cosmological z-distribution might be important.

ii) *The Two-Quasar Proximity Effect*

If two quasars are within $\sim 1°$ in the sky, and if the lower redshift (foreground) quasar is very bright, it would be possible to detect the enhanced ionization of Lyα clouds near the foreground quasar in the line of sight to the background one (B. Paczński 1987). Computing $\omega(z)$ along the lines of sight to several such "paired" QSOs, one could construct a graph like Figure 5. This would be an interesting test of the ionization model. Figure 9 may be used as a guide to determine what QSO pairs are likely to be useful for this purpose.

iii) *Cloud Velocity Widths*

Extremely high resolution spectra are needed to determine cloud velocity widths and study the distribution of clouds in N. This would allow a more reliable determination of the proximate distribution (eq. [10]). Also, it would be interesting to look for (1) correlations between N and b, and (2) possible trends of b with ω.

iv) *BL Lac Objects and Gravitationally Lensed Quasars*

In the standard model for "blazars," emissions are strongly collimated toward the observer (Blandford and Königl 1979). The two-object proximity effect could provide an observational test of this "beaming" hypothesis. If the hypothesis is correct, there should be no depletion of Lyα clouds due to blazar emissions along the line of sight to more distant objects that are near blazars on the sky, although there *should* be proximate depletion in the blazar's line of sight.

If gravitational lensing is important (in either BL Lac objects or in ordinary QSOs), Lyα cloud depletion should be reduced in comparison to that expected on the basis of apparent luminosity, both along the line of sight and perpendicular to it.

Note that proximity effect–based tests using line catalogs complete to smaller equivalent width thresholds W_t (due to improvements in instrumentation and data reduction), afford statistical certainty that increases exponentially with decreasing W_t.

We thank Edward Jenkins, Bohdan Paczyński, and the referee Hugh Murdoch for insightful comments. This research was supported by NASA grant NAGW-765 to Princeton University.

REFERENCES

Atwood, B., Baldwin, J. A., and Carswell, R. F. 1985, *Ap. J.*, **292**, 58.
Bechtold, J., Green, R. F., Weymann, R. J., Schmidt, M., Estabrook, F. B., Sherman, R. D., Wahlquist, H. D., and Heckman, T. M. 1984, *Ap. J.*, **281**, 76.
Bechtold, J., Weymann, R. J., Lin, Z., and Malkan, M. A. 1987, *Ap. J.*, **315**, 180 (BWLM).
Black, J. H. 1981, *M.N.R.A.S.*, **197**, 553.
Blades, J. C., Hunstead, R. W., Murdoch, H. S., and Pettini, M. 1985, *Ap. J.*, **288**, 580.
Blandford, R. D., and Königl, A. 1979, *Ap. J.*, **232**, 34.
Boksenberg, A., and Snijders, M. A. J. 1981, *M.N.R.A.S.*, **194**, 353.
Carr, B. J., Bond, J. R., and Arnett, W. D. 1984, *Ap. J.*, **277**, 445.
Carswell, R. F., Morton, D. C., Smith, M. G., Stockton, A. N., Turnshek, D. A., and Weymann, R. J. 1984, *Ap. J.*, **278**, 486.
Carswell, R. F., Whelan, J. A. J., Smith, M. G., Boksenberg, A., and Tytler, D. 1982, *M.N.R.A.S.*, **198**, 91.
Chen, J. S., Morton, D. C., Peterson, B. A., Wright, A. E., and Jauncey, D. L. 1981, *M.N.R.A.S.*, **196**, 715.
Evans, A., and Hart, D. 1977, *Astr. Ap.*, **58**, 241.
Green, R. F., Pier, J. R., Schmidt, M., Estabrook, F. B., Lane, A. L., and Wahlquist, H. D. 1980, *Ap. J.*, **239**, 483.
Heisler, J., and Ostriker, J. P. 1987, *Ap. J.*, submitted (HO).
———. 1988, *Ap. J.*, in press.
Hewitt, A., and Burbidge, G. 1987, *Ap. J. Suppl.*, **63**, 1.
Hunstead, R. W., Murdoch, H. S., Peterson, B. A., Blades, J. C., Jauncey, D. L., Wright, A. E., Pettini, M., and Savage, A. 1986, *Ap. J.*, **305**, 496.
Ikeuchi, S., and Ostriker, J. P. 1986, *Ap. J.*, **301**, 522.
Jenkins, E. B. 1988, in preparation.
Koo, D. C., and Kron, R. G. 1988, *Ap. J.*, **325**, 92.
Marshall, H. L. 1985, *Ap. J.*, **299**, 109.
Marshall, H. L., Avni, Y., Tananbaum, H., and Zamorani, G. 1983, *Ap. J.*, **269**, 35.
Morton, D. C., Chen, J. S., Wright, A. E., Peterson, B. A., and Jauncey, D. L. 1980, *M.N.R.A.S.*, **193**, 399.
Murdoch, H. S., Hunstead, R. W., Pettini, M., and Blades, J. C. 1986, *Ap. J.*, **309**, 19 (MHPB).
Oke, J. B., and Korycansky, D. G. 1982, *Ap. J.*, **255**, 11.
Ostriker, J. P., and Heisler, J. 1984, *Ap. J.*, **278**, 1.
Ostriker, J. P., and Vietri, M. 1985, *Nature*, **318**, 446.
Paczyński, B. 1987, private communication.
Peebles, P. J. E. 1971, *Physical Cosmology* (Princeton: Princeton University Press).
Peterson, B. A. 1978, in *IAU Symposium 79, The Large Scale Structure of the Universe*, ed. M. S. Longair and J. Einasto (Dordrecht: Reidel), p. 389.
Peterson, B. A., Chen, J. S., Morton, D. C., Wright, A. E., and Jauncey, D. L. 1984, Anglo-Australian Observatory Report 1986.
Sargent, W. L. W., Young, P. J., and Boksenberg, A. 1982, *Ap. J.*, **252**, 54.
Sargent, W. L. W., Young, P. J., Bokensberg, A., and Tytler, D. 1980, *Ap. J. Suppl.*, **42**, 41.
Sargent, W. L. W., Young, P. J., and Schneider, D. 1982, *Ap. J.*, **256**, 374.
Schmidt, M., and Green, R. F. 1983, *Ap. J.*, **269**, 352.
Schmidt, M., Schneider, D. P., and Gunn, J. E. 1986, *Ap. J.*, **310**, 518.
Shapiro, P. R. 1986, *Pub. A.S.P.*, **98**, 1014.
Smith, M. G., *et al.* 1981, *M.N.R.A.S.*, **195**, 437.
Snijders, M. A., Pettini, M., and Boksenberg, A. 1981, *Ap. J.*, **245**, 386.
Steidel, C. C., and Sargent, W. L. W. 1987, *Ap. J.*, **313**, 171.
Tytler, D. A. 1987, *Ap. J.*, **321**, 69.
Wolfe, A. M. 1987, *Phil. Trans. Roy. Soc London*, in press.
Young, P. J., Deverill, R. S., Gunn, J. E., Westphal, J. A., and Kristian, J. 1981, *Ap. J.*, **244**, 723.
Young, P. J., Sargent, W. L. W., and Boksenberg, A. 1982, *Ap. J.*, **252**, 10.

STANISLAW BAJTLIK, ROBERT C. DUNCAN, and JEREMIAH P. OSTRIKER: Princeton Astrophysical Observatory, Princeton, NJ 08544